Available online at www.sciencedirect.com
ScienceDirect
C. R. Mecanique 337 (2009) 340–351
COMPTES RENDUS MECANIQUE

Combustion for aerospace propulsion

A DES method applied to a Backward Facing Step reactive flow

B. Sainte-Rose [a,*], N. Bertier [a], S. Deck [b], F. Dupoirieux [c]

[a] *Onera, Fundamental and Applied Energetics Department, 29, avenue de la Division Leclerc, 92322 Châtillon cedex, France*
[b] *Onera, Applied Aerodynamics Department, 8, rue des Vertugadins, 92190 Meudon, France*
[c] *Onera, Fundamental and Applied Energetics Department, chemin de la Hunière, 91761 Palaiseau, France*

Available online 21 July 2009

Abstract

Hybrid Reynolds Averaged Navier Stokes–Large Eddy Simulation is a trend which is becoming of common use in aerodynamics but has seldom been employed to simulate reactive flows. Such methods, like the Delayed Detached Eddy Simulation (DDES) presented in this article, have been created to treat near wall flows with a RANS approach while switching to LES in the separated flow region. It is indeed an affordable solution to simulate complex and unsteady compressible flows and to have access to accurate skin friction and wall thermal fluxes. In order to validate this technique in combustion, we chose a simple and well documented Backward Facing Step combustor. To account for turbulent combustion a Dynamic Thickened Flame was used. The results obtained on this case show a good agreement with the experimental database and are of the same quality as LES in the separated region for both inert and reactive flows. ***To cite this article: B. Sainte-Rose et al., C. R. Mecanique 337 (2009).***

Résumé

Sur l'utilisation d'une méthode de type DES pour des écoulements réactifs. Les approches hybrides de type équations de Navier Stokes moyennées (RANS)/Simulation aux Grandes Echelles (LES) sont de plus en plus répandues dans la communauté des aérodynamiciens, en revanche elles sont très peu utilisées pour des applications en combustion. Ce type de méthodes auquel appartient la Delayed Detached Eddy Simulation (DDES) présentée dans cet article, ont été conçues pour traiter les écoulements pariétaux par une approche RANS tout en basculant vers une approche LES loin des parois. Cette modélisation permet favorablement de simuler des écoulements compressibles complexes et instationnaires tout en prenant en compte correctement les transferts pariétaux (frottement, flux de chaleur). Pour valider cette technique en combustion sur un cas simple, nous avons choisi de simuler une chambre de combustion en forme de marche descendante. Les calculs des écoulements réactifs sont effectués avec un modèle de flamme épaissie dynamique (DTF) pour modéliser la combustion turbulente. Les résultats obtenus sur ce cas sont en accord avec la base de données expérimentales et sont de la même qualité que la LES dans la zone décollée. ***Pour citer cet article : B. Sainte-Rose et al., C. R. Mecanique 337 (2009).***

Keywords: Combustion; Delayed Detached Eddy Simulation

Mots-clés : Combustion ; Delayed Detached Eddy Simulation

* Corresponding author.
E-mail address: bruno.sainte-rose@onera.fr (B. Sainte-Rose).

1631-0721/$ – see front matter
doi:10.1016/j.crme.2009.06.017

1. Introduction

The increase in computational power is allowing the use of unsteady simulation methods to study the reactive flows in combustion devices. Among them, Large Eddy Simulations (LES) are the most widely used [1]. Meanwhile, steady simulations, such as Reynolds Averaged Navier Stokes (RANS), which solve the averaged quantities of the flow are progressively narrowed to parametric studies in the design path.

In fact, LES is well suited for massively separated flows such as those encountered in swirled burners, ramjets and is effective to reproduce combustion instabilities. Indeed, LES was formulated so as to take the most energetic structures of the turbulent flow while modelling the subgrid turbulent dissipation. That is why, when most of the dynamic of the flow and the combustion process occurs in separated flow regions and no accurate resolution of the wall flows is required, LES is an efficient solution. In fact, in the separated flow area most of the turbulent scales can affordably be captured by the grid without exceeding CPU costs. However, in certain cases, an accurate resolution of the dynamics of attached boundary layers is required. We can cite, for example, massively separated and adverse pressure gradient sensitive flows like shock boundary layer interactions. In these situations it is very costly to make a LES of an attached turbulent boundary layer since the active structures encountered at low wall units, such as streaks, need a very thin refinement in the streamwise and spanwise directions and lead to prohibitive mesh sizes (typically $\Delta x^+ \approx 50$, $\Delta z^+ \approx 20$). On the other hand, a RANS simulation of an attached boundary layer is less costly since the grid refinement in these two directions can be much coarser than in the direction normal to the wall. Consequently, hybrid RANS/LES methods such as the Delayed Detached Eddy Simulation (DDES) [2] addressed in this study, are increasingly used to simulate complex configurations in aerodynamics. This model combines a RANS approach in attached boundary layers with a subgrid viscosity approach in the separated regions. Numerous studies from Onera successfully proposed this kind of approach in aerodynamics to simulate inlet [3], trailing edges [4] and airfoils [5].

However, these methods, to the author's knowledge, have been used for reactive flows only to describe the non-premixed combustion in a scramjet [6] but only on a two-dimensional case. Hence, they could be very relevant both to give a better description of the aerodynamics of reactive flows (shock-boundary layer interaction in spaceship overexpanded nozzles for example) and to make accurate calculations of wall thermal fluxes and friction in reactive cases.

The aim of this study is to present how a DDES approach can be applied to the study of combustion in the Onera CEDRE code for energetics. The features of a Backward Facing Step combustor are indeed well suited to validate the DDES approach proposed in this paper. In fact, it combines attached boundary layers and a massive separated region in which the mixing between fresh and hot gases results in a turbulent flame.

This article is organized as follows. First, the numerical methods and physical models are presented with a particular attention to the DDES approach. In a second part, a description of the test case and the basic physics of such flow will be introduced along with the conditions of our computations. The results of our simulations both for inert and reactive flows for the three approaches RANS, LES and DDES will finally be presented and discussed.

2. Description of the numerical methods and physical models

2.1. General description

The code for energetics CEDRE[1] developed at Onera is used on a wide range of applications to describe various physical situations (gaseous or dispersed phase, influence of radiative transfer, etc.). The code solves the mass, momentum, species and total energy conservation equations as well as transport equations for turbulent (RANS) or subgrid (LES) viscosity, chemical species and other useful quantities. The numerical method is based on a cell-centered finite volume approach for general unstructured grids. Roe's flux difference splitting, associated with a MUSCL approach, is employed for the advective fluxes. This method results in a second order spatial accuracy (third order on an isotropic mesh). The time integration is carried out using a second order sub-iterated Gear scheme [7]. The specific modellings used for turbulence and for turbulent combustion are detailed in the next sub-sections.

[1] Calcus d'écoulements diphasiques réactifs pour l'énergetique.

2.2. Turbulence modelling

First, let us be reminded of the general principle of Detached Eddy Simulation which was originally introduced by Spalart et al. [8] (DES97). If we consider a simplified approach towards turbulence modelling, the turbulent viscosity ν_t, whatever of RANS or LES can be formalized as $u \times l$ where u and l are respectively the characteristic fluctuating velocity and length scale. In a RANS approach, l is model dependent whereas in LES using a subgrid scale approach, l scales as $C\Delta$ where Δ is the filter width which is of the same magnitude as the mesh scale and C is a constant. Considering the two approaches to estimate l, the RANS/LES method is introduced. The formulation originally proposed for DES97 suggests to take [8]:

$$l_{DES} = \min(l_{RANS}, C_{DES}\Delta) \tag{1}$$

Nevertheless, a special concern was devoted to the region named the grey area where the model switches from RANS to LES. The treatment of this region needs a careful monitoring and has motivated the improvement of the original method leading to the introduction of DDES. Indeed, while the DES97 length scale depends only on the mesh spacing and on l_{RANS} resulting in a grid-dependent switching region, the DDES ensures that boundary layers are included in the RANS region avoiding an early switch to LES which can lead to unphysical outcomes like artificial relaminarization, also called Modelled Stress Depletion [9]. A new length scale l_{DDES} is thus proposed in [2] and verifies:

$$l_{DDES} = l_{RANS} - f_{DDES} \times \max(0, l_{RANS} - C_{DES}\Delta) \tag{2}$$

Therefore, the purpose of the function f_{DDES} is to shield the boundary layer since it is equal to 0 in the boundary layer and 1 elsewhere. On a theoretical ground, all RANS models can be efficiently derived into (D)DES according to the previous guidelines [10].

In the current paper we use a DDES approach based on the $k-\omega$ SST model [13] which was originally derivated into DES97 by Strelets [12]. Let us consider the source term, S_k, of the turbulent kinetic energy k given by the SST model [11]:

$$S_k = P_k - \varepsilon \tag{3}$$

In Eq. (3) P_k and ε stand respectively for the production and destruction term of the turbulent kinetic energy. The modification introduced by the DDES approach only affects the destruction term ε which is thus modified:

$$\varepsilon = \beta^*\omega k = \frac{k^{3/2}}{l_{RANS}} \longrightarrow \frac{k^{3/2}}{l_{DDES}} \tag{4}$$

The production term is given by:

$$P_k = 2\tilde{S}_{ij}\tilde{S}_{ij}\frac{k}{\omega} \tag{5}$$

where $\tilde{\mathbf{S}}$ is the symmetric part of tensor $\nabla\tilde{\mathbf{u}}$. One can verify in Eq. (4) that $l_{RANS} = \sqrt{k}/(\beta^*\omega)$.

In addition, specific modifications were proposed to the original DDES approach: in the reference paper, Δ is equal to $\max(\Delta_x, \Delta_y, \Delta_z)$ which was first proposed for DES97 whereas, in our case, we take Δ equal to the cubic root of the mesh volume where $Volume = \Delta_x\Delta_y\Delta_z$; this definition which was also used in the Extended DDES approach found in [14] proves to be less dissipative and closer to the LES formulation in the separated flow area. Moreover, in this paper we take $f_{DDES} = 1 - F_1$, where F_1 is a specific function used in the SST model to yield the boundary layers to the $k-\omega$ branch of the SST model [11]. The use of this function was proposed for the SST based DES [15]. The value of the parameter β^* is equal to 0.09. The subgrid parameter C_{DES} is defined as:

$$C_{DES} = (1 - F_1)C_{DES}^{k-\varepsilon} + F_1 C_{DES}^{k-\omega} \tag{6}$$

where $C_{DES}^{k-\varepsilon} = 0.61$ and $C_{DES}^{k-\omega} = 0.78$ as for the Strelets formulation [12]. From Eq. (2) and as illustrated in Fig. 1, one can notice that classical DES stands for $f_{DDES} = 1$, and that $f_{DDES} = 0$ obtained near the wall yields to RANS equations. Far from the wall, if the destruction balances the production term in Eq. (3) then the eddy viscosity $\nu_t = k/\omega$ reduces to:

$$\nu_t = \beta^{*3/2} {C_{DES}^{k-\varepsilon}}^2 \Delta^2 (2\tilde{S}_{ij}\tilde{S}_{ij})^{1/2} \tag{7}$$

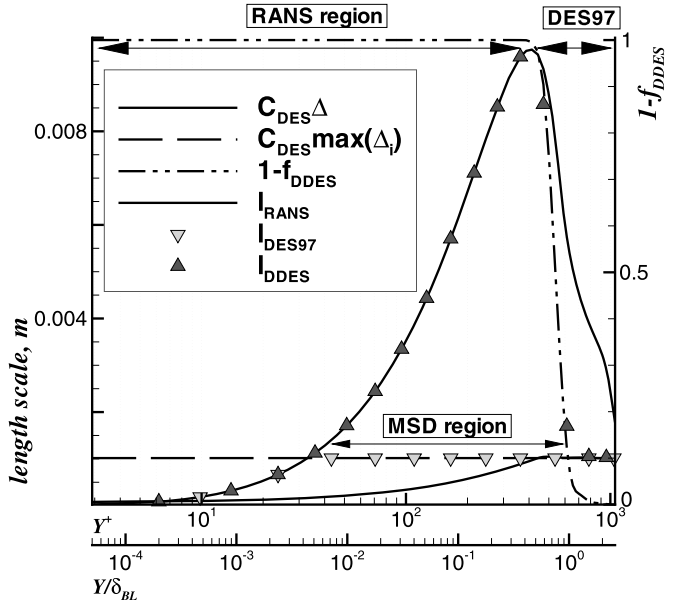

Fig. 1. Evolution of l_{DDES}, l_{DES97}, $1 - f_{DDES}$ in a boundary layer along with two different definitions of the mesh scale.

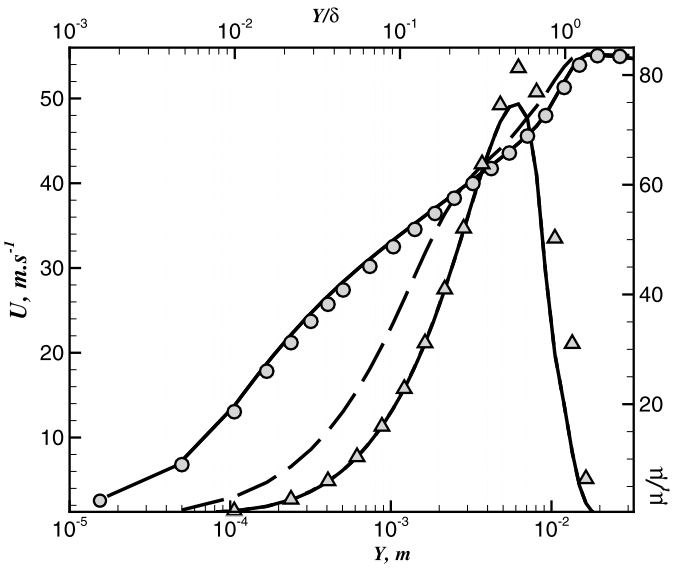

Fig. 2. Streamwise velocity profiles comparison between SGS approach (dashed), DDES (solid) and RANS (symbols), ν_t/ν is displayed for RANS and DDES.

This eddy viscosity adopts the form a Smagorinsky approach [16] where the subgrid scale viscosity is expressed as $\nu_{SGS} = (2\tilde{S}_{ij}\tilde{S}_{ij})^{1/2}(C_{SGS}\Delta)^2$. According to the constants of the SST RANS model, the corresponding value of $C_{SGS} \approx 0.1$. This expression must not hold when we are close to the wall because the grid spacing in the boundary layers is not suited to LES and would lead to laminarization. In the boundary layers DDES leads to a RANS expression of the turbulent viscosity so that, if we compare the velocity profiles obtained in the vicinity of the lower wall of the BFS intake channel (Fig. 2), one can notice that the SGS viscosity approach suffers from a poor estimation of the friction whereas DDES and RANS profiles are perfectly matched for an attached boundary layer.

Two other approaches are compared to the DDES computations. Firstly DDES is compared to the LES approach including a slightly modified Smagorinsky model [17]:

$$\nu_{SGS} = (2\tilde{S}_{ij}\tilde{S}_{ij})^{1/2}(C_{SGS}\breve{\Delta})^2 \tag{8}$$

where $\breve{\Delta} = \min(\Delta, 0.4d_w/C_{SGS})$ to make sure that ν_{SGS} reduces to zero at the wall, with d_w the distance to the wall and C_{SGS} equal to 0.1 to match with the DDES approach in the separated region. A more specific wall modelling such as Wall-Adapting Local Eddy Viscosity [18] should have given a better description of the boundary layer than the current LES approach but the implementation of such a model in our computation tools is out of the scope of this work. Secondly, DDES has been compared with the RANS approach including the usual SST model.

2.3. Combustion modelling

The modelling used in this work for turbulent combustion is the Thickened Flame Model for LES (TFLES). It gives indeed access to the accurate laminar flame speed by thickening the flame front [19] of a factor F – which is mesh dependent – to allow more points in the flame front on coarse grids; in the meantime the interaction with turbulence is modelled thanks to an efficiency function E proposed by Colin et al. [20] which accounts for the non-resolved wrinkling of the flame front and the modelled subgrid scales. These two terms appear in the aerothermochemical equations: the laminar thermal and diffusive fluxes are multiplied by EF resulting in thickening the flame front, while the species source terms are multiplied by E/F. In its original version, the modifications proposed above affect the species balance equations in the whole computational domain, which results in overestimating the diffusive fluxes far from the flame front. In our case we are interested in wall flows and in particular in thermal fluxes in the near wall region which could not be correctly calculated because of the modification of the diffusion coefficients. As a consequence, a dynamic formulation is used [21]. Its aim is to limit the thickening process to the flame front by introducing a flame sensor. In the case of the premixed methane–air flame studied in the following section, the source terms $\dot{\omega}_\alpha$ resulting from the chemical reaction appearing in the mass balances are obtained by using an Arrhenius law with a one step chemical mechanism of Westbrook and Dryer [22].

3. Presentation of the simulated experiment and of the calculation conditions

3.1. General features of the A3C combustor

The main features of this test case which make it suitable for a validation of the DDES approach are, as illustrated in Fig. 3:

- Two attached boundary layers in the upstream channel which have to be treated in RANS;
- Downstream of the step, a shear layer develops and will allow us to appraise of the quality of the LES content of the DDES model and its ability to account for the development of the turbulent flame;
- The size of the recirculating bubble and the reattachment point is also a good criterion to value the efficiency of our method.

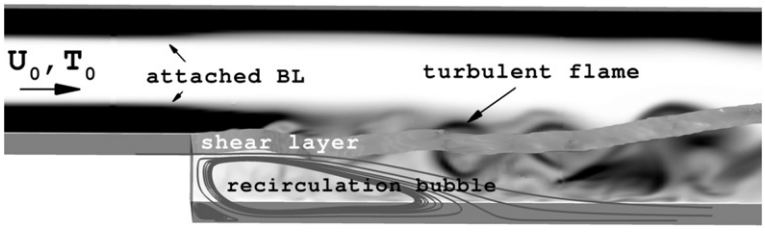

Fig. 3. Sketch of the BFS reactive flow.

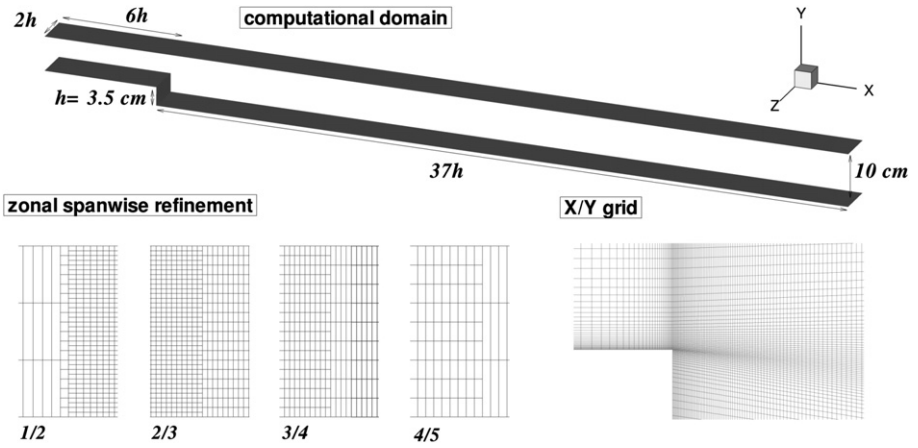

Fig. 4. (from top to bottom, counterclockwise): 3D view of the computational domain, focus on the zonal refinement in the (x, z) plane, zoom in the corner of the 2D grid.

Table 1
2D grid refinement.

Zone	n_x	n_y	y_0 (m), y_0/δ_{BL}
Inlet channel	63	71	lower wall: 5×10^{-5}, 4×10^{-3} – upper wall: 4×10^{-4}, 8×10^{-2}
Chamber	626	115	lower wall: 5×10^{-5}, 4×10^{-3} – upper wall: 4×10^{-4}, 8×10^{-2}

Our current BFS case was introduced in the frame of the A3C[2] (1980–1990s) and MICAEDI[3] (2000s) programs led by Onera [23]. The experimental database includes velocity measurements made using Laser Doppler Velocimetry (LDV). Coherent Anti-Stokes Raman Spectroscopy (CARS) was used to measure the temperature of the reactive flow.

3.2. Presentation of the numerical test case

3.2.1. Mesh generation

At first, we have to define the computational domain (see Fig. 4 for details). The geometrical features and measures are detailed in Fig. 4. The height of the step is $h = 3.5$ cm. The length of the upstream channel (6 h) was chosen so as to allow the upstream boundary layers to develop and to limit the influence of the inlet conditions on the separated region downstream of the step. The downstream channel measures 37 h which should allow a proper description of the complete flame of which the average attachment point to the upper wall is located about 23 h downstream of the step. In the spanwise direction, the experimental size of the chamber is of 0.1 m which corresponds to 2.86 h. Given the computational cost of the resolution of the lateral boundary layers, we preferred to simulate a width of 2 h with periodic boundary conditions to get the accurate development of the 3D shear layer.

Secondly let us now describe the meshing strategy used on this case. The length of the downstream channel is of 37 h, whereas the zone where the physics of the flow require a thin spanwise resolution measures about 8.5 h, which corresponds to about 1.5 times the recirculation mean length for the inert case. Consequently, we focus our meshing effort on the region close to the step in our meshing strategy. The flexibility of our code enables us to locally refine the calculation grid by introduction of structured blocks including any number of smaller cells. The (x, y) grid whose characteristics are displayed in Table 1, was generated so as to verify $y_0^+ < 3$ with 25 points in the lower wall boundary layers, and $y_0^+ \approx 18$ with 15 points in the upper wall boundary layer (low Reynolds approach is used to treat this boundary layer). These values are the minimum required (low pressure gradient) to predict the accurate skin friction on the lower wall and behavior in the vorticity thickness downstream of the step. In the separated flow region

[2] Concerted Action for Combustion Chamber.
[3] Program on Combustion Instabilities.

Table 2
Operating conditions.

U_0	T_0	Φ	Re_h	P_0
50 m s^{-1}	520 K	0.8	40,000	100, 400 Pa

Table 3
Summary of the computations.

Inert case	dt (μs)	T (s)	grid	Reacting case	dt (μs)	T (s)	grid
DDES a/b	2.5	0.2	II/I	DDES	1.5	0.2	II
LES	2.5	0.2	II	LES	1.5	0.2	II
RANS			2D	RANS			2D

the grid yields a 2D isotropic (n_x, n_y) region. Concerning the spanwise refinement, 5 zones are distributed in the streamwise direction (as shown in Fig. 4):

- from the inlet to $X/h = -1$, $n_z = 3$ and $\Delta_z/\delta_{BL} = 1.8$;
- from $X/h = -1$ to $X/h = +8$, $n_z = 18$ (grid I) or 36 (grid II) and $\Delta_z/\delta_{BL} = 0.3$ or 0.15;
- from $X/h = +8$ to $X/h = +18.5$, $n_z = 18$; from $X/h = +18.5$ to $X/h = +31.4$, $n_z = 9$ and $\Delta_z/\delta_{BL} = 0.6$;
- from $X/h = +31.4$ to the outlet, $n_z = 3$.

This distribution will allow us to obtain a refined calculation grid, in the spanwise direction, only in the step region where it is required. This results in computational grid sizes of: 76,463 cells for the 2D grid, 1,072,584 cells for the 3D grid I, and 1,485,774 cells for the 3D grid II.

3.2.2. Boundary conditions and summary of the computations

The general operating conditions retained for our computations are detailed in Table 2. For the inlet conditions, a velocity profile is imposed at the entrance of the channel so as to obtain a boundary layer thickness of 1.3 cm at the step. Due to lack of information we impose Dirichlet conditions at the entrance without fluctuations. This approximation will affect the level of turbulence in the upper part of the chamber and may lead to an underestimation the flame angle. In the outlet section the pressure is applied using non-reflecting NSCBC boundary conditions [24]. The upper and lower walls are taken adiabatic since no measurements of the wall temperature were completed.

The computations presented in this article are organized as gathered in Table 3. Concerning the combustion model, note that a single Arrhenius law was employed for the RANS computations of the reactive flow. The time step for our unsteady computations was chosen so as to verify a maximum Courant Friedrichs Lewy number of 12 when based on the pressure wave speed, i.e. when $CFL = \mathrm{d}t(|\mathbf{u}| + c)/\Delta$ and 0.6 when based on the convective speed, i.e. when $CFL = \mathrm{d}t|\mathbf{u}|/\Delta$. With these CFL levels a good accuracy of the implicit time integration can be expected.

4. Results and discussion

4.1. Analysis of the inert flow

4.1.1. Instantaneous flow fields

On the lower part of Fig. 5, the instantaneous turbulent structures are evidenced by showing a positive iso-value of Q criterion ($Q(h/U_0)^2 = 0.2$). Let us be reminded that the Q quantity is used to define the vortex tube regions which are the points where:

$$Q = \frac{1}{2}(\Omega_{ij}\Omega_{ij} - S_{ij}S_{ij}) > 0 \tag{9}$$

where $\tilde{\mathbf{S}}$ and $\tilde{\Omega}$ are, respectively, the symmetric and antisymmetric tensor of $\nabla\mathbf{u}$. One can notice in this figure the planar behavior of the structures near the step, that are typical of a Kelvin–Helmholtz instability. The 2D structures are rapidly replaced by large three-dimensional structures developing as the shear layer approaches reattachment. Note

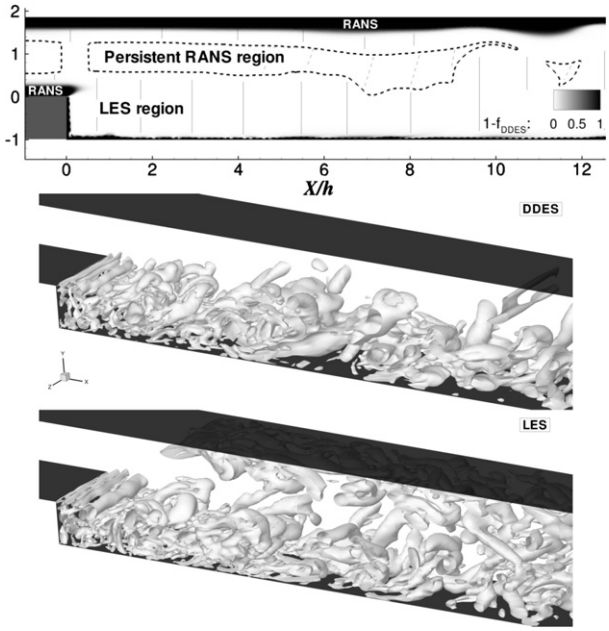

Fig. 5. (top) Distinction between RANS and LES zones for the DDES approach; (bottom) coherent structures downstream of the step using the iso-surface of $Q \times (h/U_0)^2 = 0.2$ on grid II.

Table 4
Comparison between computational results and experimental for L_r/h.

	LDV	DDES a)	DDES b)	LES	RANS
L_r/h	$4.3 < - < 6$	5.1	5.3	4.1	7.8

also the occurrence of large scale hairpin vortices in the reattachment zone. If we compare the instantaneous flow fields resulting from DDES and LES approaches, we can point out the multiplicity of the structures on the upper separated region for the LES calculation. On the upper part of the figure, we display the different regions corresponding to either RANS or LES mode of the DDES approach. The particular definition of the RANS length scale leads to a persisting RANS region that will further be discussed for the computations of the reactive flow.

4.1.2. Statistical fields

The time-dependent field is averaged in time during the calculation. The first analysis of the recirculating zone which can be made on our computations concerns the reattachment length. The ratio between the mean reattachment length and the size of the step L_r/h is compared to the experimental value in Table 4. One can notice that the mean reattachment length is in a better agreement with the experiment for the DDES computations than for LES and is clearly overestimated for RANS. Moreover we can notice that the velocity profiles in the lower recirculating region are in good agreement with the experimental values (Fig. 7) for both LES and DDES whereas the RANS computations show more discrepancies. Concerning the upper wall, the LES gives rise to an upper recirculation (Fig. 6) which is not experimentally observed. Indeed, the grid refinement near the wall is too coarse in the spanwise and in the streamwise direction to make possible a good description of the boundary layer by the subgrid viscosity approach which is laminarized.

Concerning the *rms* fluctuating streamwise velocity u'_{rms}, Fig. 7 also illustrates the quality of the shear layer description for DDES computations on the first four profiles. The influence of the mesh refinement is also illustrated for the DDES computations; indeed, while it does not affect much the averaged velocity it obviously deteriorates the development of the shear layer as displayed at $X/h = 1.1,\ 2.3$. Further downstream, the shear layer expansion is slightly overestimated; a possible explanation could be the numerical dissipation induced by the coarser spanwise refinement which lead to an overestimated coherence of the shear layer structures. The comparison with the LES results

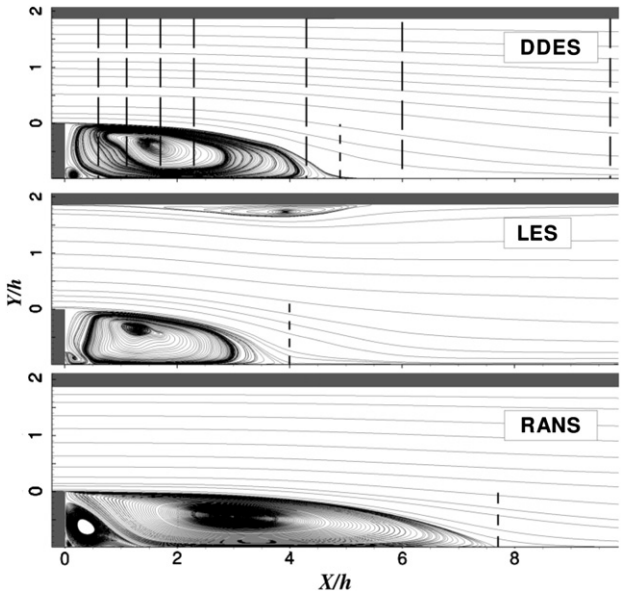

Fig. 6. Streamlines for the averaged computations and location of the LDV diagnosis (long dash) for DDES, LES on grid II and 2D-RANS, the reattachment point is evidenced with the small dashed line (from top to bottom).

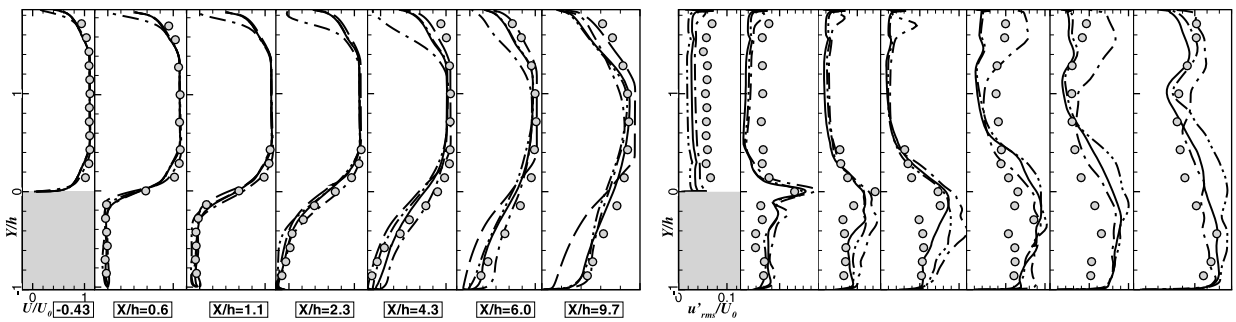

Fig. 7. (left) Averaged streamwise velocity U and (right) *rms* fluctuations u'_{rms} normalized by U_0: DDES a), solid lines; DDES b), dash double dots; LES, dash dots; RANS, long dashes.

underlines the effect of the quasi-laminarized nature of the upstream boundary layers, penalizes and overestimates the velocity fluctuations.

4.2. Analysis of the reactive flow

4.2.1. Instantaneous flowfields

As in Fig. 5, iso-surfaces of the Q criterion are displayed for the unsteady computations of the reactive flow in the lower part of Fig. 8. An iso-surface of temperature $T = 1500$ K allows one to approximately locate the instantaneous position of the flame front. From this figure, it appears that the shape of the flame is mostly affected by the turbulence model close to the step. In the LES computation, the multiplicity of vortices which are convected in the channel result in an important wrinkling of the flame. The upper part of the figure evidences the fact that a part of the flame is located in a region where the DDES model is in the RANS mode while the combustion model is adapted to LES. Further work is required to quantify this effect after adaptation of the combustion model.

4.2.2. Statistical fields

The averaged results for 2D-RANS, LES and DDES computations for velocity are presented first. The experimental and numerical recirculation lengths are compared in Table 5. For these three computations, the recirculation bubble

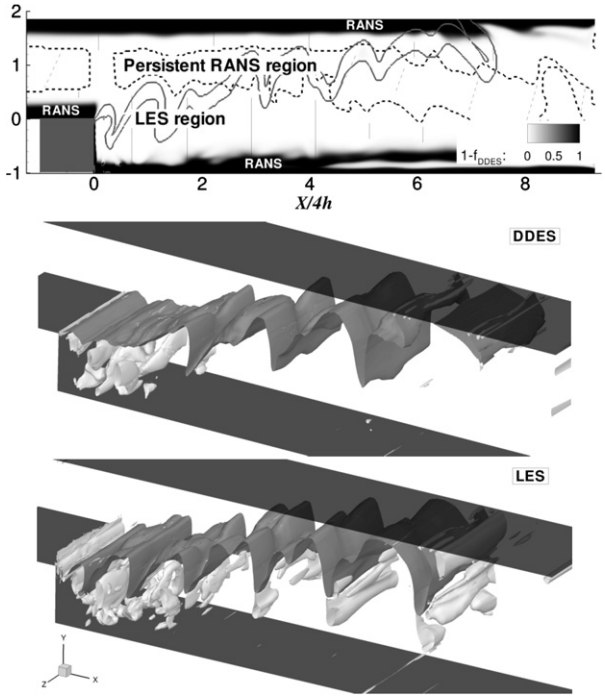

Fig. 8. (top) Distinction between RANS and LES zones for the DDES approach; (bottom) coherent structures downstream of the step using the iso-surface of $Q \times (h/U_0)^2 = 0.3$, position of the flame using an iso-surface of $T = 1500$ K, for convenience the aspect ratio is 1:4:4.

Table 5
Comparison between computational results and experimental for the averaged size of the bubble.

	LDV	DDES	LES	2D-RANS
L_r/h	$2.9 < - < 3.4$	3.8	3.6	4.7

is overestimated. Averaged streamlines for these three computations are also provided in Fig. 9, the use of the DDES approach clearly improves the resolution of the bubble compared to the 2D-RANS approach. Moreover, the results obtained in the separated flow region show a very good agreement with the LDV measurements for both LES and DDES in Fig. 10. Similarly to the inert computations, the fluctuating velocities are quite overestimated by the LES which explains the important wrinkling observed previously.

Let us now consider the results obtained for the averaged temperature flowfield. In Fig. 11, an iso-line of $T = 1500$ K is displayed for our three computations and compared to the measurements. This layout allows us to approximately locate the averaged computed flame. The results obtained close to the step for DDES and LES are very satisfying since the flame angle is well reproduced whereas the RANS clearly underestimates the flame angle. The higher levels of velocity fluctuations for the LES computations can explain the upper position of the flame. However, further downstream more discrepancies are evidenced. In fact, the flame structure is rather bi-dimensional close to the step whereas it becomes more tri-dimensional close to reattachment where the spanwise grid spacing avoids an accurate resolution of the dynamics of the flow (in the LES sense).

If we now have a look at the temperature profiles in Fig. 12, the previous remarks concerning the position of the flame is therefore verified since we observe that the peak and the levels found for the fluctuating temperature are in very good agreement with the experiments except for the first profile for which the need to characterize of the thermal conditions at the lower wall is highlighted. As for the temperature fluctuations, the value of $T' = \sqrt{\overline{T^2} - \overline{T}^2}$ is shown in the same figure. The difference between LES and DDES discussed previously is identified since the important wrinkling leads to an overestimation of the flame brush in the first three profiles.

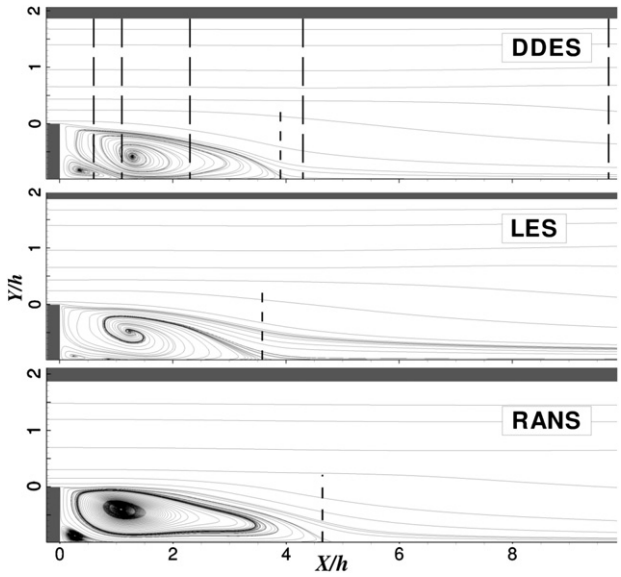

Fig. 9. Streamlines for the averaged computations and location of the LDV diagnosis (long dash) for DDES, LES and 2D-RANS, the reattachment point is evidenced with the small dashed line (from top to bottom).

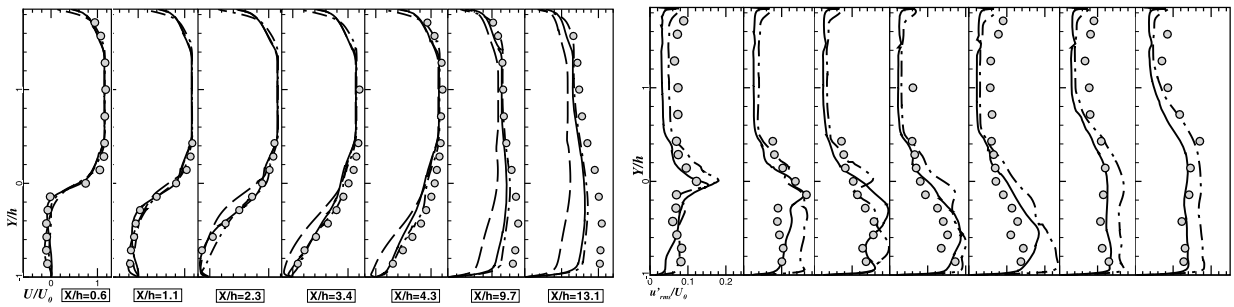

Fig. 10. (left) Averaged streamwise velocity U and (right) *rms* fluctuations u'_{rms} normalized by U_0: DDES, solid lines; LES, dash dots; RANS, long dashes.

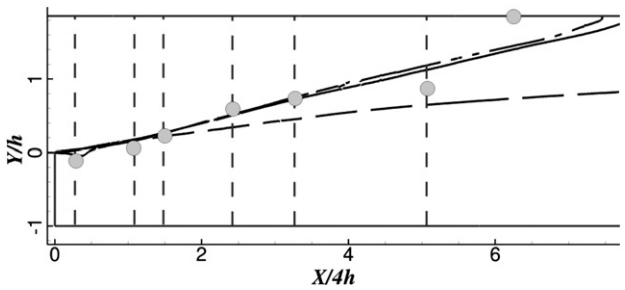

Fig. 11. 1500 K temperature iso-line for DDES (solid), LES (dash-dot), RANS (dashed), CARS (circles).

5. Conclusion

A DES approach has been proposed to treat combustion problems requiring a fine evaluation of wall flows and attached boundary layers, either to have access to the precise skin friction or thermal fluxes or to cope with pressure gradient-sensitive flows. In fact, this hybrid RANS/LES model has been conceived to treat the attached boundary layers with a RANS model while switching to a subgrid viscosity formulation away from solid walls.

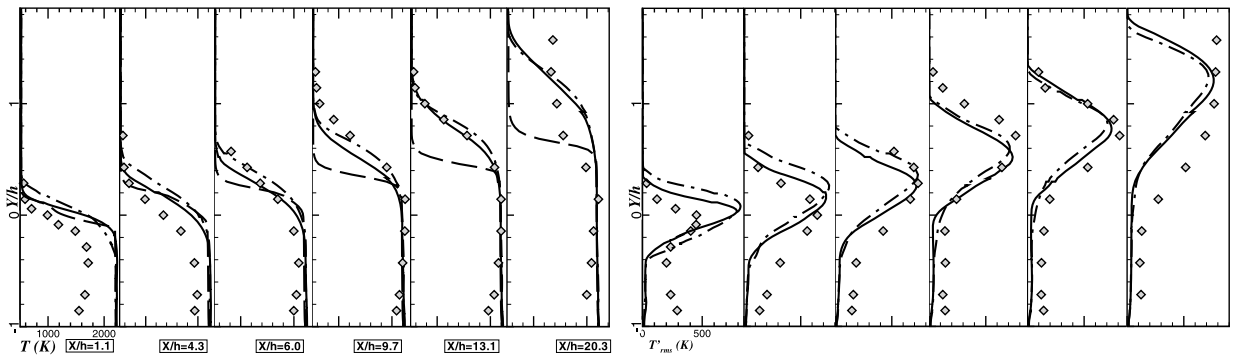

Fig. 12. Mean and fluctuating temperature T and T' DDES (solid), LES (dash-dot) and RANS (dashed only for T), CARS measurements (diamonds).

The study of an inert and reactive flow behind a BFS has been presented for validation purpose. DES and particularly DDES addressed in this article have been compared to RANS and LES with a SGS approach. Concerning the combustion modelling, a DTF was employed "as is" both for LES and DDES.

First, the inert computations have highlighted the improvement of DDES compared to RANS but also the known limitations of the LES method employed. An inaccurate evaluation of the skin friction with the SGS approach indeed leads to an unphysical separation on the upper wall. Second, the description of the turbulent flame has proven to be as efficient for both LES and DDES. Compared to the RANS computations, the mixing introduced by the LES mode of the DDES has provided a significant improvement. Finally, limitations linked to the use of different length scales between LES and DDES motivate a further adaptation of the combustion model and will follow the present work.

Acknowledgements

The authors gratefully acknowledge the CNES (Centre Nationale d'Etudes Spatiales) for the funding of B. Sainte-Rose PhD studies.

References

[1] T. Poinsot, D. Veynante, Theoretical and Numerical Combustion, R.T. Edwards Ed., 2001.
[2] P.R. Spalart, S. Deck, M.L. Shur, K.D. Squires, M.Kh. Strelets, A. Travin, Theor. Comput. Fluid Dyn. 20 (2006) 181–195.
[3] S. Trapier, S. Deck, P. Duveau, AIAA J. 46 (2008) 118–203.
[4] F. Simon, S. Deck, P. Guillen, P. Sagaut, A. Merlen, J. Fluid Mech. 591 (2007) 215–253.
[5] S. Deck, AIAA J. 43 (2005) 1556–1566.
[6] J.-Y. Choi, F. Ma, V. Yang, AIAA 2005-4428, 2005.
[7] T.H. Pulliam, AIAA 93-660, 1993.
[8] P.R. Spalart, W.-H. Jou, M.Kh. Strelets, S.R. Allmaras, AFOSR (1997) 137–147.
[9] P. Sagaut, S. Deck, M. Terracol, Multiscale and Multiresolution Approaches in Turbulence, Imperial College Press, 2006.
[10] P.R. Spalart, Annu. Rev. Fluid Mech. 41 (2009) 181–202.
[11] F.R. Menter, AIAA 1993-2906, 1993.
[12] M.Kh. Strelets, AIAA 2001-0879, 2001.
[13] B. Sainte-Rose, N. Bertier, S. Deck, F. Dupoirieux, AIAA 2008-5134, 2008.
[14] J. Riou, E. Garnier, S. Deck, C. Basdevant, AIAA J. 42 (2009) 345–360.
[15] F.R. Menter, M. Kuntz, R. Langtry, in: 4th Symposium on Turbulence Heat and Mass Transfer, 2003.
[16] J. Smagorinsky, M. Weather Rev. 91 (1963) 99–165.
[17] N. Bertier, Ph.D. thesis, Universite Paris 6, 2006.
[18] F. Nicoud, F. Ducros, Flow Turbul. Combust. 62 (1999) 183–200.
[19] T.D. Butler, P.J. O'Rourke, in: 16th International Symposium on Combustion, 1976.
[20] O. Colin, F. Ducros, D. Veynante, T. Poinsot, Phys. Fluids 12 (7) (2000) 1843–1863.
[21] J.P. Legier, T. Poinsot, D. Veynante, in: Proceedings of the Center for Turbulence Research, 2000, pp. 157–168.
[22] C.K. Westbrook, F.L. Dryer, Combust. Sci. Technol. 2 (1981) 31–43.
[23] P. Moreau, J. Labbe, F. Dupoirieux, R. Borghi, in: 5th Symposium on Turbulence and Shear Flow, 1985.
[24] T. Poinsot, S. Lele, J. Comput. Phys. 101 (1992) 104–129.